Journal of Porous Media, 20(1): 1–17 (2017)

HEAT AND MASS TRANSFER CHARACTERISTICS OF Al_2O_3–WATER AND Ag–WATER NANOFLUID THROUGH POROUS MEDIA OVER A VERTICAL CONE WITH HEAT GENERATION/ABSORPTION

P. Sudarsana Reddy[1,*] & Ali J. Chamkha[2,3]

[1]*Department of Mathematics, RGM College of Engineering and Technology, Nandyal 518501, AP, India*

[2]*Mechanical Engineering Department, Prince Mohammad Bin Fahd University, Al-Khobar 31952, Saudi Arabia*

[3]*Prince Sultan Endowment for Energy and Environment, Prince Mohammad Bin Fahd University, Al-Khobar 31952, Saudi Arabia*

*Address all correspondence to: P. Sudarsana Reddy, E-mail: suda1983@gmail.com

Original Manuscript Submitted: 8/31/2015; Final Draft Received: 5/12/2016

In this article, we have presented a numerical solution to the MHD heat and mass transfer flow of a nanofluid through porous media over a vertical cone with heat generation/absorption, thermal radiation, and chemical reaction. Though we have different varieties of nanofluids, we have considered Al_2O_3–water and Ag–water based nanofluids (with volume fraction 1% and 4%) in this problem. The transformed conservation equations for the nanofluid are solved numerically subject to the boundary conditions using an efficient, extensively validated, variational finite element analysis. The numerical code is validated with previous studies. The influence of important nondimensional parameters, namely, nanoparticle volume fraction (φ), Prandtl number (Pr), magnetic parameter (M), mixed convection (Ra), buoyancy ratio (Nr), and space-dependent (A), temperature-dependent (B), thermal radiation (R), and chemical reaction (Cr) on velocity, temperature, and nanoparticle concentration fields as well as the skin-friction coefficient, Nusselt number, and Sherwood number are examined in detail and the results are shown graphically and in tabular form to illustrate the physical importance of the problem.

KEY WORDS: *heat and mass transfer, Al_2O_3–water and Ag–water nanofluid, MHD, thermal radiation, chemical reaction, finite element method*

1. INTRODUCTION

A nanofluid is a fluid containing small volumetric quantities of nanometer-sized particles (1–100 nm), called nanoparticles. These fluids are engineered in a suspension of nanometer-sized solid particles or fibers in conventional base fluids like water, ethylene glycol, toluene, and engine oil. The nanoparticles used in nanofluids are typically made of metals (Al, Cu), oxides (Al_2O_3, CuO, TiO_2, SiO_2), carbides (SiC), nitrides (AlN, SiN), or nonmetals (graphite, carbon nanotubes). In recent years, the concept of a nanofluid has been proposed as route for enhancing the performance of the heat transfer rates in liquids. Low thermal conductivity is a primary limitation in the development of energy-efficient heat transfer fluids. Conventional heat transfer fluids such as water, ethylene glycol, and engine oil have limited heat transfer capabilities due to their low heat transfer properties. In contrast, metals have thermal conductivities up to three times higher than these fluids, so it is naturally desirable to combine the two substances to produce a heat transfer medium that behaves like a fluid but has the thermal properties of a metal. The materials

1091–028X/17/$35.00

NOMENCLATURE

A	space-dependent heat source/sink
a	constant
B	temperature-dependent heat source/sink
B_0	magnetic field strength
C_f	skin-friction coefficient
Cr	chemical reaction parameter
D_m	mean fluid concentration
$f(\eta)$	dimensionless stream function
g	gravitational acceleration
Jw	wall mass flux
K	permeability parameter
K_r	rate of chemical reaction
k_s	thermal conductivity of nanoparticle
K^*	mean absorption coefficient
M	magnetic parameter
Nr	buoyancy ratio parameter
Nu_x	Nusselt number
P	pressure
Pr	Prandtl number
q_r	radiative heat flux
q_w	wall heat flux
q'''	nonuniform heat source/sink
R	radiation parameter
Ra	mixed convection parameter
Sc	Schmidt number
Sh_x	Sherwood number
T_w	temperature at the cone surface
T_∞	ambient temperature attained

Greek Symbols

α	thermal diffusivity of base fluid
β	thermal expansion coefficient
η	similarity variable
k_{nf}	thermal conductivity of nanofluid
$(\mu)_{nf}$	viscosity of the nanofluid
ν_f	kinematic viscosity of the base fluid
φ	nanoparticle volume fraction
$\phi(\eta)$	dimensionless nanoparticle volume fraction
ϕ_w	nanoparticle volume fraction on the cone
ϕ_∞	ambient nanoparticle volume fraction
$(\rho)_f$	density of the base fluid
ρ_p	nanoparticle mass density
$(\rho c_p)_f$	heat capacitance of the base fluid
$(\rho c_p)_{nf}$	heat capacitance of the nanofluid
ψ	stream function
σ	electrical conductivity
σ^*	Stephan–Boltzmann constant
τ	parameter defined by $\varepsilon[(\rho c)_p/(\rho c)_f]$
τ_w	shear stress
$\theta(\eta)$	dimensionless temperature

Subscripts

f	base fluid
nf	nanofluid
w	condition at cone surface
∞	condition far away from cone surface

which are in nanometer size possess unique physical and chemical properties. They can flow smoothly through microchannels without clogging because they are sufficiently small to behave similarly to liquid molecules. This fact has attracted much research into the investigation of the heat transfer characteristics in nanofluids. It has been found that the presence of nanoparticles increases the thermal conductivity of the base fluid in the range of 15%–40%. Effective cooling techniques are much needed in many industries such as manufacturing, power, transportation, electronic devices, and, in particular, the next generation of thin-film solar energy collector devices.

We can find many experimental and numerical studies in literature to know the importance of nanofluid natural convection heat transfer (Wang and Mujumdar, 2008; Sarkar, 2011; Kamyar et al., 2012). However, we can witness diverse conclusions in those experimental and numerical investigations (Haddad et al., 2012). In an experimental investigation of nanofluid natural convection heat transfer, deterioration was usually noticed, whereas in numerical investigation, enhancement is reported. In his benchmark study, Buongiorno (2006) has reported seven possible mechanisms associating nanofluid natural convection through moment of nanoparticles in the base fluid using scale analysis. These mechanisms are nanoparticle size, inertia, particle agglomeration, Magnus effect, volume fraction of the nanoparticle, Brownian motion, thermophoresis, and so on. Putra et al. (2003) have found heat transfer depreciation in both Al_2O_3–water and CuO–water based nanofluids (with volume fraction 1% and 4%) in their experimental study. Wen and Ding (2005) also reported heat transfer deterioration in TiO_2–water based nanofluids

(with volume fraction 0.19% and 0.57%) in their study. Li and Peterson (2010) have described natural convection heat transfer deceleration in the Al_2O_3–water based nanofluid (with volume fraction 0.5% and 6%), and because of nanoparticle Brownian motion, smoothing the temperature gradient causes delay in natural convection. Rui et al. (2011) noticed deterioration in natural convection heat transfer in the Al_2O_3–water based nanofluid and due to mass diffusion of nanoparticles in their experimental study under the Rayleigh–Benard configuration. Nnanna (2007) have found in their experiment that the natural convection heat transfer depreciates when nanoparticle volume fraction is more than 2% in the Al_2O_3–water based nanofluid owing to an increase in kinematic viscosity. Ho et al. (2010) also conveyed up to 18% natural convective heat transfer improvement in Al_2O_3–water nanofluid (with volume fraction 0.1%), but deterioration was found when the volume fraction was more than 2%.

Eastman et al. (1997) have noticed in their numerical study that the thermal conductivity of the base fluid (water) is increased up to 60% when CuO nanoparticles of volume fraction 5% are added to the base fluid. This is because of increasing surface area of the base fluid due to the suspension of nanoparticles. Eastman et al. (2001) have also showed that the thermal conductivity is increased 40% when copper nanoparticles of volume fraction less than 1% are added to ethylene glycol or oil. Choi et al. (2001) have reported that there is 150% enhancement in thermal conductivity when carbon nanotubes are added to ethylene glycol or oil. In addition, Xie et al. (2002) have observed that Al_2O_3–ethylene glycol based nanofluid thermal conductivity is increased in the range 25%–30%. Recently, Bresme and Oettel (2007) and Lervik et al. (2009) have presented numerical studies to analyze the possible heat transfer mechanisms between nanoparticle and fluid. Eliodoro and Pietro (2011) have analyzed surface heat transfer enhancement by carbon nanofins. In this study, they have proposed nanofins are the alternative to nanofluids. Eliodoro et al. (2014) have analyzed the scaling analysis for the water passage through nanoconfined geometries. However, today, normal computational fluid dynamics (CFD) investigation is still playing a dominant role in this area. Khanafer et al. (2003) found remarkable heat transfer enhancement in CuO–water based nanofluids when nanoparticle volume fraction is up to 20%. Oztop and Abu-Nada (2008) have discussed heat and mass transfer characteristics of Al_2O_3–water, TiO_2–water, and CuO–water nanofluids over two-dimensional rectangular enclosures and found significant natural heat transfer enhancement when volume fraction of nanoparticles is up to 20%. Aminossadati and Ghasemi (2009) reported that adding copper (Cu), silver (Ag), Al_2O_3, and TiO_2 nanoparticles (φ was up to 20%) could improve the cooling performance of pure water in a bottom-heated two-dimensional enclosure, especially when the Rayleigh number was low. Ghasemi and Aminossadati (2010) have noticed remarkable enhancement in the rates of heat transfer in CuO–water nanofluid with volume fraction (φ) $1\% \sim 4\%$ in a two-dimensional triangular enclosure. Fakhreddine Segni et al. (2011) found nanofluid natural heat convection enhancement in Al_2O_3, TiO_2, and Cu nanoparticles when the volume fraction of nanoparticles is less than 5% in a two-dimensional cavity. Ternik and Rudolf (2012) examined the heat transfer enhancement of water-based gold (Au), Al_2O_3, Cu, and TiO_2 nanofluids when φ was up to 10% in a two-dimensional cavity. Recently, Chamkha and colleagues (Chamkha et al., 2012, 2013; Chamkha and Rashad, 2014) have presented mixed convection heat and mass transfer characteristics of nanofluid under different geometries, like wedge, cone, and rotating vertical cone, by taking magnetic field, radiation, and other parameters. Rashad et al. (2014) have analyzed natural convection non-Darcy nanofluid over a vertical cone through a porous medium. Very recently, Sheremet and Pop (2014) have reported natural convection of nanofluid in a square porous cavity using Buongiorno's mathematical model. Sheremet et al. (2015a) noticed three-dimensional natural convection in a porous enclosure filled with a nanofluid using Buongiorno's mathematical model. Sheremet et al. (2015b,c) have conferred the Tiwari and Das' model of nanofluid through a porous medium over a square cavity and a cubical cavity, respectively.

Magnetic nanoparticles are especially useful in biomedicine, sink float separation, cancer therapy, and so on. Specific biomedical applications involving nanofluids include hyperthermia, magnetic cell separation, drug delivery, and contrast enhancement in magnetic resonance imaging. Thermal radiation plays a very significant role in the surface heat transfer when convection heat transfer is very small. It has applications in manufacturing industries for the design of reliable equipment, nuclear plants, gas turbines, and various propulsion devices for aircraft, missiles, satellites, and space vehicles. Also, the effects of thermal radiation on forced and free convection flow are important in the context of space technology and processes involving high temperatures. The working fluid heat generation or absorption effects are very crucial in monitoring the heat transfer in the regions, heat removal from nuclear fuel debris, underground disposal of radioactive waste material, storage of foodstuffs, and exothermic chemical reactions

and dissociating fluids in packed-bed reactors. This heat source can occur in the form of a coil or battery. In addition, in many chemical engineering processes, chemical reactions take place between a foreign mass and the working fluid, which moves due to the stretching of the surface. The order of the chemical reaction depends on many factors. First-order chemical reaction is one of the simplest reactions in which the rate of reaction is directly proportional to the species concentration. In view of the preceding applications, Chamkha (2003) has analyzed magnetohydrodynamic (MHD) steady state heat and mass transfer flow over a uniformly moving vertical surface with first-order chemical reaction and heat generation/absorption. Amit and Mahesh Kumar (2014) have discussed MHD convection of nanofluids through porous media. EL-Kabeir et al. (2015) have presented mixed convection flow of nanofluids over a solid sphere through a porous medium under convective boundary conditions by taking thermal radiation into account. Representative studies in this area may be found in the articles by Ellahi and colleagues (Ellahi, 2013; Ellahi et al., 2012, 2013, 2015a,b), Noreen Sher et al. (2014a,b, 2015), Rashidi et al. (2015), Sheikholeslami et al. (2014a,b,c, 2015a,b), Sheikholeslami and Ellahi (2015), and Zeeshan et al. (2014).

To the best of the authors' knowledge, no studies have been found in literature concerning the influence of nanoparticle volume fraction on Al_2O_3–water and Ag–water based nanofluids over a vertical cone througha porous medium with magnetic field, chemical reaction, radiation, and heat generation/absorption. Hence, the problem is addressed in this article. The problem presented here has many industrial, transportation, electronics, and biomedical applications, such as in advanced nuclear systems, cylindrical heat pipes, automobiles, fuel cells, drug delivery, biological sensors, and hybrid-powered engines.

2. MATHEMATICAL FORMULATION

Figure 1 demonstrates a two-dimensional, steady, electrically conducting heat and mass transfer boundary layer flow of nanofluid over a vertical cone. The coordinate system is chosen as the x-axis is coincident with the flow direction over the cone surface. It is assumed that T_w and ϕ_w are the temperature and nanoparticle volume fraction at the surface of the cone ($y = 0$) and T_∞ and ϕ_∞ are the temperature and nanoparticle volume fraction of the ambient fluid, respectively. An external magnetic field of strength B_0 is applied in the direction of the y-axis. The thermophysical properties of the nanofluid are given in Table 1. By considering the work of Kuznetsov and Nield (2010) and by employing the Oberbeck–Boussinesq approximation, the governing equations describing the steady state conservation of mass, momentum, energy, and conservation of nanoparticles for nanofluids in the presence of thermal radiation and other important parameters take the following form:

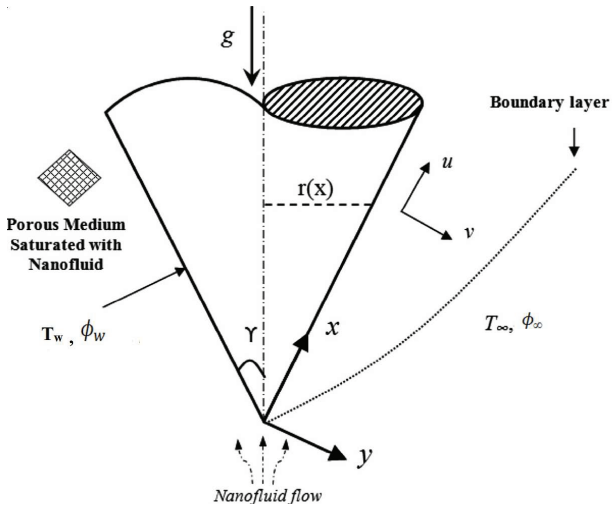

FIG. 1: Physical model and coordinate system

TABLE 1: Thermophysical properties of water and nanoparticles

Fluid	**ρ (Kg/m^3)**	C_p **(J/kg K)**	k **(W/mK)**	**β$\times$ 10^5 (K^{-1})**
Pure water	997.1	4179	0.613	21
Copper (Cu)	8933	385	401	1.67
Silver (Ag)	10500	235	429	1.89
Alumina (Al_2O_3)	3970	765	40	0.85
Titanium oxide (TiO_2)	4250	686.2	8.9538	0.9

$$\frac{\partial(ru)}{\partial x}+\frac{\partial(rv)}{\partial y}=0 \tag{1}$$

$$u\frac{\partial u}{\partial x}+v\frac{\partial u}{\partial y}=\frac{\mu_{nf}}{\rho_{nf}}\frac{\partial^2 u}{\partial y^2}-\frac{\mu_{nf}}{\rho_{nf}}\frac{1}{K}u+g\left[\beta\left(T-T_\infty\right)-\beta^*\left(\phi-\phi_\infty\right)\right]\cos\gamma-\frac{\sigma B_0^2}{\rho_{nf}}u \tag{2}$$

$$u\frac{\partial T}{\partial x}+v\frac{\partial T}{\partial y}=\alpha_{nf}\frac{\partial^2 T}{\partial y^2}+\frac{1}{\left(\rho c_p\right)_{nf}}(q''')-\frac{1}{\left(\rho c_p\right)_{nf}}\frac{\partial q_r}{\partial y} \tag{3}$$

$$u\frac{\partial \phi}{\partial x}+v\frac{\partial \phi}{\partial y}=D_m\frac{\partial^2 \phi}{\partial y^2}-K_r(\phi-\phi_\infty) \tag{4}$$

The associated boundary conditions are

$$u=0,\quad v=0,\quad T=T_w,\quad \phi=\phi_w\quad \text{at}\quad y=0 \tag{5}$$

$$u\to 0,\quad T\longrightarrow T_\infty,\quad \phi\longrightarrow\phi_\infty\quad \text{at}\quad y\to\infty \tag{6}$$

The radiative heat flux q_r (using Rosseland approximation) is defined as

$$q_r=-\frac{4\sigma^*}{3K^*}\frac{\partial T^4}{\partial y} \tag{7}$$

We assume that the temperature variances inside the flow are such that the term T^4 can be represented as linear function of temperature, so it has Taylor series expansion. After neglecting higher-order terms from the Taylor series expansion of T^4 about T_∞, we get

$$T^4\cong 4{T_\infty}^3T-3T_\infty^4 \tag{8}$$

Thus substituting Eq. (8) in Eq. (7), we get

$$q_r=-\frac{16T_\infty^3\sigma^*}{3K^*}\frac{\partial T}{\partial y} \tag{9}$$

The nonuniform heat source/sink, q''', is defined as

$$q'''=\frac{\kappa_f}{x\nu_f}\left[A1\left(T_w-T_\infty\right)f'+B1\left(T-T_\infty\right)\right]$$

where $A1$ and $B1$ are the coefficients of space and temperature-dependent heat source/sink, respectively. The case $A1>0$, $B1>0$ corresponds to an internal heat source and the case $A1<0$, $B1<0$ corresponds to an internal heat sink.

The dynamic viscosity μ_{nf}, density ρ_{nf}, thermal diffusivity α_{nf}, thermal conductivity k_{nf}, and heat capacitance $\left(\rho c_p\right)_{nf}$ of the nanofluid and kinematic viscosity ν_f of the base fluid are defined as follows:

$$\alpha_{nf}=\frac{k_{nf}}{\left(\rho c_p\right)_{nf}},\quad \mu_{nf}=\frac{\mu_f}{(1-\varphi)^{2.5}},\quad \nu_f=\frac{\mu_f}{\rho_f},\quad \rho_{nf}=(1-\varphi)\rho_f+\varphi\rho_s,$$

$$(\rho c_p)_{nf} = (1-\varphi)(\rho c_p)_f + \varphi(\rho c_p)_s, \quad k_{nf} = k_f\left(\frac{k_s + 2k_f - 2\varphi(k_f - k_s)}{k_s + 2k_f + 2\varphi(k_f - k_s)}\right)$$

We now introduce the following similarity variables to transform the governing equations into a system of ordinary differential equations:

$$\psi = \sqrt{a\nu_f}\, x\, f(\eta), \quad u = axf'(\eta), \quad v = -\sqrt{a\nu_f}\, f(\eta)$$

$$\eta = \sqrt{\frac{a}{\nu_f}}\, y, \quad \theta(\eta) = \frac{T - T_\infty}{T_w - T_\infty}, \quad S(\eta) = \frac{\phi - \phi_\infty}{\phi_w - \phi_\infty} \tag{10}$$

Here r can be approximated by the local radius of the cone, if the thermal boundary layer is thin, and is related to the x coordinate by $r = x\sin\gamma$.

Substituting Eq. (10) into Eqs. (1)–(4), we get the following system of nonlinear ordinary differential equations:

$$f''' + A_1\left[f f'' - (f')^2 - \frac{M}{A_2}f'\right] - k_1 f' + A_1\,\mathrm{Ra}[\theta - Nr\,S] = 0 \tag{11}$$

$$(1+R)\,\theta'' + \mathrm{Pr}A_3\,A_4\,f\,\theta' + A_4(A f' + B\theta) = 0 \tag{12}$$

$$S'' + \mathrm{Sc}\,f\,S' - \mathrm{Sc}.Cr.S = 0 \tag{13}$$

The transformed boundary conditions are

$$\eta = 0, \quad f = 0, \quad f' = 1, \quad \theta = 1, \quad S = 1, \quad \eta \longrightarrow \infty, \quad f' = 0, \quad \theta = 0, \quad S = 0 \tag{14}$$

where prime denotes differentiation with respect to η and the significant thermophysical parameters dictating the flow dynamics are defined by

$$Nr = \frac{\beta^*(\phi_w - \phi_\infty)}{\beta(T_w - T_\infty)}, \quad k_1 = \frac{\nu_f}{Ka}, \quad \mathrm{Ra} = \frac{g\beta(T_w - T_\infty)\cos(\gamma)}{a^2 x}, \quad Cr = \frac{K_r}{a}, \quad \mathrm{Pr} = \frac{\nu_f}{\alpha_f}$$

$$R = \frac{16T_\infty^3\sigma^*}{3K^*k}, \quad M = \frac{\sigma\beta_o^2}{a\,\rho_f}, \quad \mathrm{Sc} = \frac{\nu_f}{D_m}, \quad A = \frac{A1}{a\,x}, \quad B = \frac{B1}{a\,x}, \quad A_1 = (1-\varphi)^{2.5}\left[(1-\varphi) + \varphi\left(\frac{\rho_s}{\rho_f}\right)\right],$$

$$A_2 = (1-\varphi) + \varphi\left(\frac{\rho_s}{\rho_f}\right), \quad A_3 = (1-\varphi) + \varphi\left(\frac{(\rho C_p)_s}{(\rho C_p)_f}\right), \quad A_4 = \frac{k_f}{k_{nf}}$$

Quantities of practical interest in this problem are skin-friction coefficient, local Nusselt number Nu_x, and local Sherwood number Sh_x, which are defined as

$$C_f = \frac{2\tau_w}{\rho U_\infty^2}, \quad \mathrm{Nu}_x = \frac{xq_w}{k(T_w - T_\infty)}, \quad \mathrm{Sh}_x = \frac{xJ_w}{D_{\mathbf{B}}(\phi_w - \phi_\infty)} \tag{15}$$

The set of ordinary differential equations (11)–(13) are highly nonlinear and therefore cannot be solved analytically. The finite-element method (FEM) (Bhargava et al., 2009; Anwar Bég et al., 2008; Rana and Bhargava, 2012; Reddy and Chamkha, 2016) has been implemented to solve these nonlinear equations. The very important aspect in this numerical procedure is to select an approximate finite value of η_∞. So, to estimate the relevant value of η_∞, the solution process has been started with an initial value of η_∞ = 4, and then Eqs. (11)–(13) are solved together with boundary conditions (14). We have updated the value of η_∞ and the solution process is continued until the results are not affected with further values of η_∞ The choice of $\eta_{\max}$ = 6 and $\eta_{\max}$ = 8 for velocity and temperature concentration has confirmed that all the numerical solutions approach the asymptotic values at the free-stream conditions.

3. NUMERICAL METHOD OF SOLUTION

3.1 The Finite-Element Method

The FEM is a powerful method for solving ordinary differential equations and partial differential equations. The basic idea of this method is dividing the whole domain into smaller elements of finite dimension called finite elements. This method is a good numerical method in modern engineering analysis, and it can be applied for solving integral equations including heat transfer, fluid mechanics, chemical processing, electrical systems, and many other fields. The steps involved in the FEM are as follows:

1. *Finite-element discretization*. The whole domain is divided into a finite number of subdomains, which is called the discretization of the domain. Each subdomain is called an element. The collection of elements is called the finite-element mesh.

2. *Generation of the element equations.*

    a. From the mesh, a typical element is isolated and the variational formulation of the given problem over the typical element is constructed.

    b. An approximate solution of the variational problem is assumed, and the element equations are made by substituting this solution in the above system.

    c. The element matrix, which is called the stiffness matrix, is constructed by using the element interpolation functions.

3. *Assembly of element equations*. The algebraic equations so obtained are assembled by imposing the interelement continuity conditions. This yields a large number of algebraic equations known as the global FEM, which governs the whole domain.

4. *Imposition of boundary conditions*. The essential and natural boundary conditions are imposed on the assembled equations.

5. *Solution of assembled equations*. The assembled equations so obtained can be solved by any of the numerical techniques, namely, the Gauss elimination method, LU decomposition method, and so on. An important consideration is the shape functions employed to approximate actual functions.

4. RESULTS AND DISCUSSION

The system of equations (11)–(13) together with the boundary conditions (14) are solved for different values of the parameters that describe the flow characteristics and the results are illustrated graphically in Figs. 2–10. In most practical situations, heat should be detached from the hot surface into the ambient space, so it is worth mentioning that a cone with hot surface is more practical than one with a cold surface. However, there are some cases in which there is a heat reaction or heat-absorbing process inside the cone in which the cone should be heated from the ambient space. Hence the main aim of the present study is to discuss the heat and mass transfer characteristics of nanofluid over a cone with a hot surface. Comparison with previously published work is made and is shown in Table 2.

The effects of magnetic field parameter (M) on the velocity, temperature, and concentration profiles are depicted in Figs. 2(a)–2(c) for both Al_2O_3–water and Ag–water based nanofluids. The velocity profile impedes throughout the boundary layer with the increase in the strength of magnetic parameter in both the Al_2O_3–water and Ag–water nanofluids. This is due to the fact that the presence of a magnetic field in the flow creates a force known as the Lorentz force, which acts as a retarding force, and consequently, the momentum boundary layer thickness decelerates throughout the flow region [Fig. 2(a)]. We define the thermal energy as the additional force which drags the nanofluid from the influence of the magnetic field. This additional force increases the thickness of the thermal boundary layer so that the temperature profile enriches with a rise in M, and this rise is less in the Al_2O_3–water nanofluid than in

TABLE 2: Comparison of $-f''(0)$, $-\theta'(0)$ with previously published data for Pr = 6.2, k_1 = 0, $R = 0$, Ra = 0, $Nr = 0$, Sc = 0, $A = 0$, $B = 0$, $Cr = 0$

$-f''(0)$						$-\theta'(0)$			
Parameter		**Hamad (2011)**		**Present Study**		**Hamad (2011)**		**Present Study**	
M	φ	Al_2O_3	TiO_2	Al_2O_3	TiO_2	Al_2O_3	TiO_2	Al_2O_3	TiO_2
0	0.05	1.00538	1.01150	1.00657	1.01167	1.62246	1.63791	1.62258	1.63832
	0.10	0.99877	1.00952	1.01002	1.01032	1.49170	1.51959	1.49187	1.51984
	0.15	0.98185	0.99603	0.98954	0.99666	1.37543	1.41359	1.37561	1.41386
	0.20	0.95592	0.97259	0.95601	0.97294	1.27118	1.31805	1.27153	1.31856
0.5	0.05	1.20441	1.20953	1.20481	1.20961	1.57888	1.59455	1.57892	1.59484
	0.10	1.17548	1.18463	1.17592	1.18502	1.45299	1.48124	1.45312	1.48162
	0.15	1.13889	1.15114	1.13924	1.15183	1.34103	1.37962	1.34128	1.37981
	0.20	1.09544	1.11002	1.09601	1.10857	1.24063	1.28795	1.24152	1.28814
1.0	0.05	1.37493	1.37941	1.37463	1.37982	1.54154	1.55735	1.54179	1.55758
	0.10	1.32890	1.33700	1.32902	1.33721	1.41942	1.44788	1.41991	1.44795
	0.15	1.27677	1.28771	1.27707	1.28793	1.31088	1.34974	1.31092	1.34987
	0.20	1.21910	1.23222	1.22018	1.23235	1.21360	1.26123	1.21385	1.26154
2.0	0.05	1.66436	1.66806	1.66404	1.66814	1.47841	1.49438	1.47865	1.49457
	0.10	1.59198	1.59875	1.59221	1.59880	1.36212	1.39085	1.36265	1.39096
	0.15	1.51534	1.52457	1.51563	1.52459	1.25899	1.29818	1.25913	1.29861
	0.20	1.43480	1.44596	1.43507	1.44605	1.16675	1.21474	1.16693	1.21498

the Ag–water nanofluid [Fig. 2(b)]. From Fig. 2(c), we notice that as the value of M increases, the concentration distributions are also enriched in the flow regime in both nanofluids.

The velocity, temperature, and concentration distribution for various values of the mixed convection parameter Ra is shown in Figs. 3(a)–3(c). We have observed that as the values of Ra enhance, the velocity distributions in both the Al_2O_3–water and Ag–water nanofluids elevate in the boundary layer region. This is because of the fact that convection currents improve whenever Ra increases, so that the hydrodynamic boundary layer thickness increases. It is analyzed that both temperature and concentration profiles in the Al_2O_3–water and Ag–water nanofluid impedes with increasing values of mixed convection parameter Ra. This is because of the fact that the mixed convection parameter is more dominant as compared to the buoyancy ratio parameter, so that there is retardation in the thickness of thermal and nanoparticle concentration boundary layers. Furthermore, temperature and concentration profiles increase when Ra $= 0$ (forced convection) because of no buoyancy forces, and both profiles retard with the increasing values of Ra.

Figures 4(a)–4(c) depict the velocity (f'), temperature (θ), and concentration (S) distributions for different values of the buoyancy ratio parameter (Nr). From Fig. 4(a) we noticed retardation in the thickness of hydrodynamic boundary layers in both Al_2O_3–water and Ag–water nanofluids with the higher values of Nr. The temperature profiles of the fluid increase with increasing values of buoyancy ratio parameter. This is from the reality that a higher buoyancy ratio parameter enhances the fluid temperature, so that the thermal boundary layer thickness is increased [Fig. 4(b)]. The concentration profiles also enhance throughout the fluid region for different increasing values of buoyancy ratio parameter Nr. This is because of the fact that the nanoparticle concentration boundary layer thickness in both Al_2O_3–water and Ag–water nanofluid elevates with increasing values of Nr [Fig. 4(c)].

Figures 5(a)–5(c) show the velocity (f'), temperature (θ), and concentration (S) distributions for different values of the nanoparticle volume fraction parameter (φ) for both Al_2O_3–water and Ag–water nanofluids. It is observed that the velocity profiles of both nanofluids along the cone increase with higher values of φ. The temperature and

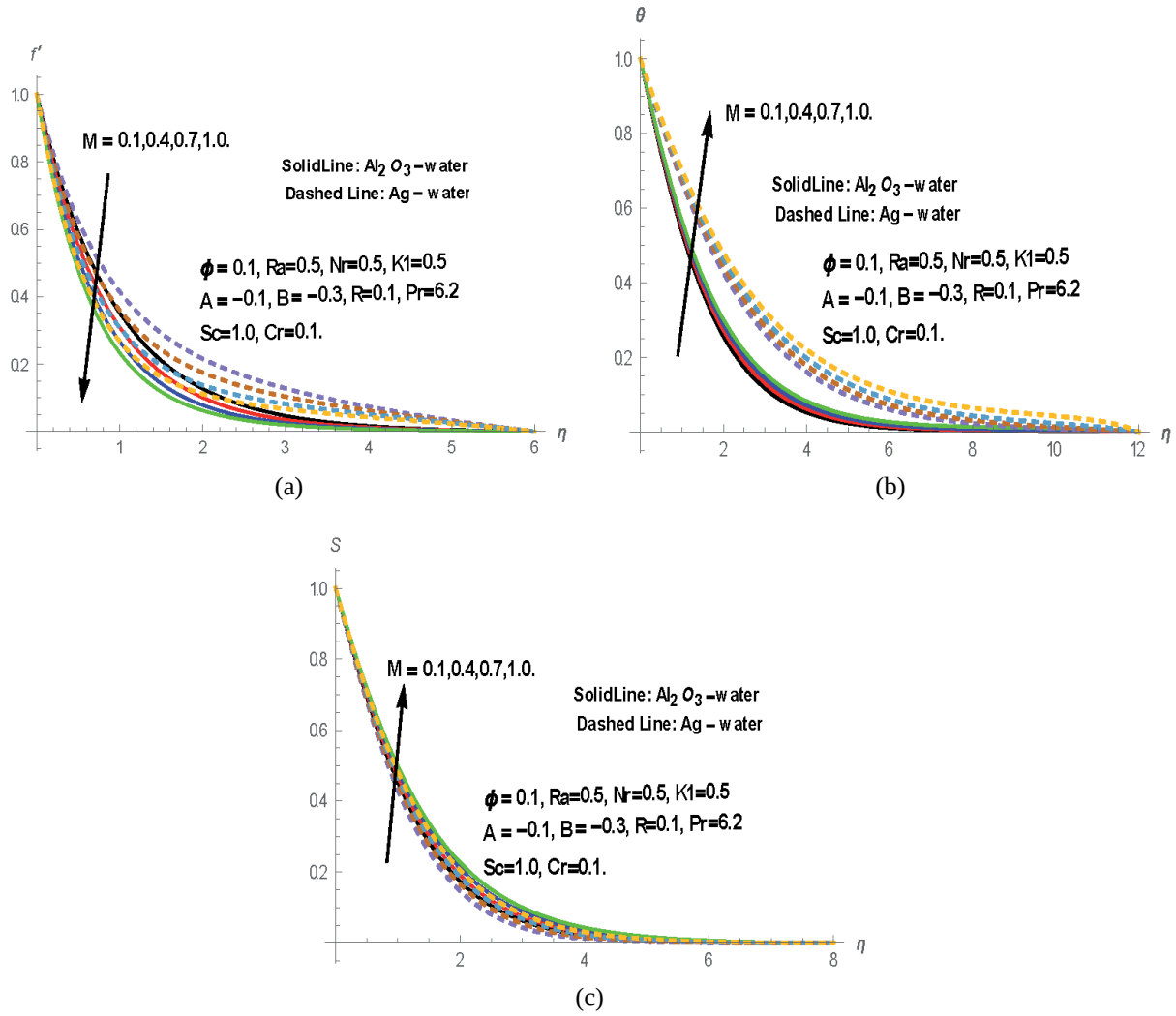

FIG. 2: Effect of M on (a) velocity, (b) temperature, and (c) concentration profiles

concentration distributions decelerate with the increasing values of φ in the Al_2O_3–water and Ag–water nanofluids. This means both the thermal and solutal boundary layer thickness is reduced in the fluid regime.

The effect of the radiation parameter (R) on velocity and temperature profiles is shown in Figs. 6(a,b) for both Al_2O_3–water and Ag–water nanofluid, respectively. It is seen that as the values of the thermal radiation parameter increase, the thermal boundary layer thickness is enhanced in both nanofluids [Fig. 6(a)]. This is due to the fact that the presence of the thermal radiation effect increases the temperature of the fluid in the entire flow region. In general, this is true because increasing the Rosseland diffusion approximation for radiation enhances the temperature of the fluid, and this increase is lower in the Al_2O_3–water nanofluid than in the Ag–water nanofluid [Fig. 6(b)].

The temperature and concentration distributions for various values of the Prandtl number (Pr) are depicted in Figs. 7(a,b). The temperature profiles decelerate with the higher Prandtl number values in both nanofluids. By definition, the Prandtl number is defined as the ratio of momentum diffusivity to the thermal diffusivity, and therefore increasing the values of Pr means a higher momentum diffusivity or a lesser thermal diffusivity, which causes the reduction in the thermal boundary layer thickness, and the deceleration in the temperature profiles is lower in the Ag–water nanofluid than in the Al_2O_3–water nanofluid [Fig. 7(a)]. We observe from Fig. 7(b) that increasing values of

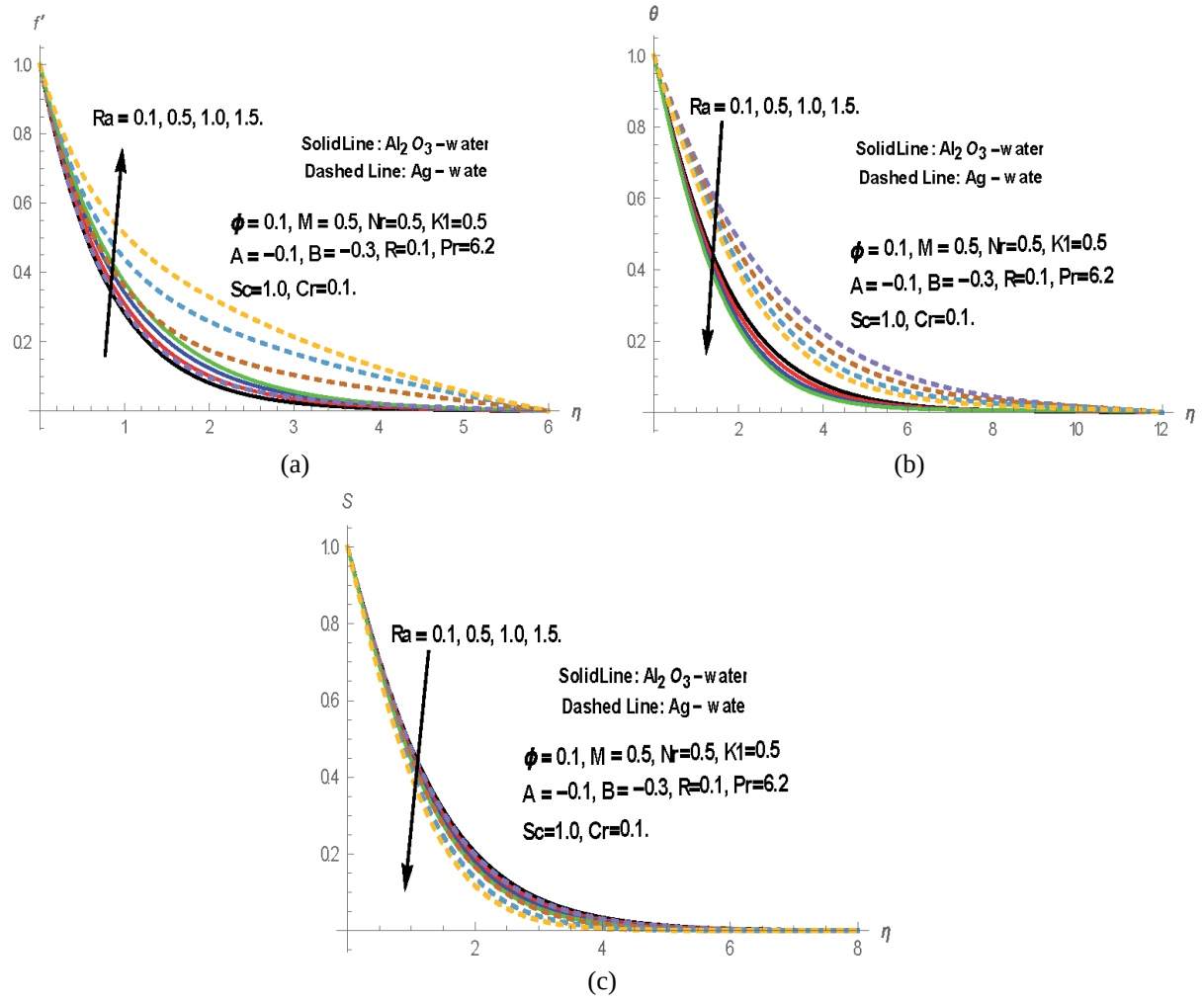

FIG. 3: Effect of Ra on (a) velocity, (b) temperature, and (c) concentration profiles

Prandtl number lead to an increase in the concentration profiles in both Al_2O_3–water and Ag–water based nanofluids. This is due to the fact that the solutal boundary layer thickness is increased with the enhancement in the values of Pr.

The temperature and concentration profiles of the Al_2O_3–water and Ag–water nanofluids for different values of the space-dependent and temperature-dependent coefficients (A and B) for a heat source/sink are depicted in Figs. 8(a,b) and 9(a,b), respectively. It is observed that temperature in the thermal boundary layer increases with increase in A and B (positive values), whereas the thermal boundary layer thickness decelerates with the decrease in the heat absorption parameters A and B (negative values). This is due to the fact that, with an increase in $A > 0$, $B > 0$ (heat source), the boundary layer creates energy, which causes the rise in the temperature profiles, whereas, with a decrease in $A < 0$, $B < 0$ (heat absorption), the boundary layer absorbs the energy so that the thermal boundary layer thickness decreases in the fluid regime, as shown in Figs. 8(a) and 9(a). The concentration profiles depreciate with A and B for both heat generation and heat absorption cases and are plotted in Figs. 8(b) and 9(b).

Figure 10 illustrates the effect of the chemical reaction parameter (Cr) on the concentration distributions for both Al_2O_3–water and Ag–water nanofluid. We see from this figure that the concentration profiles are highly influenced and impeded with the chemical reaction parameter (Cr) in the flow region, whereas there is no remarkable change in the velocity and temperature profiles.

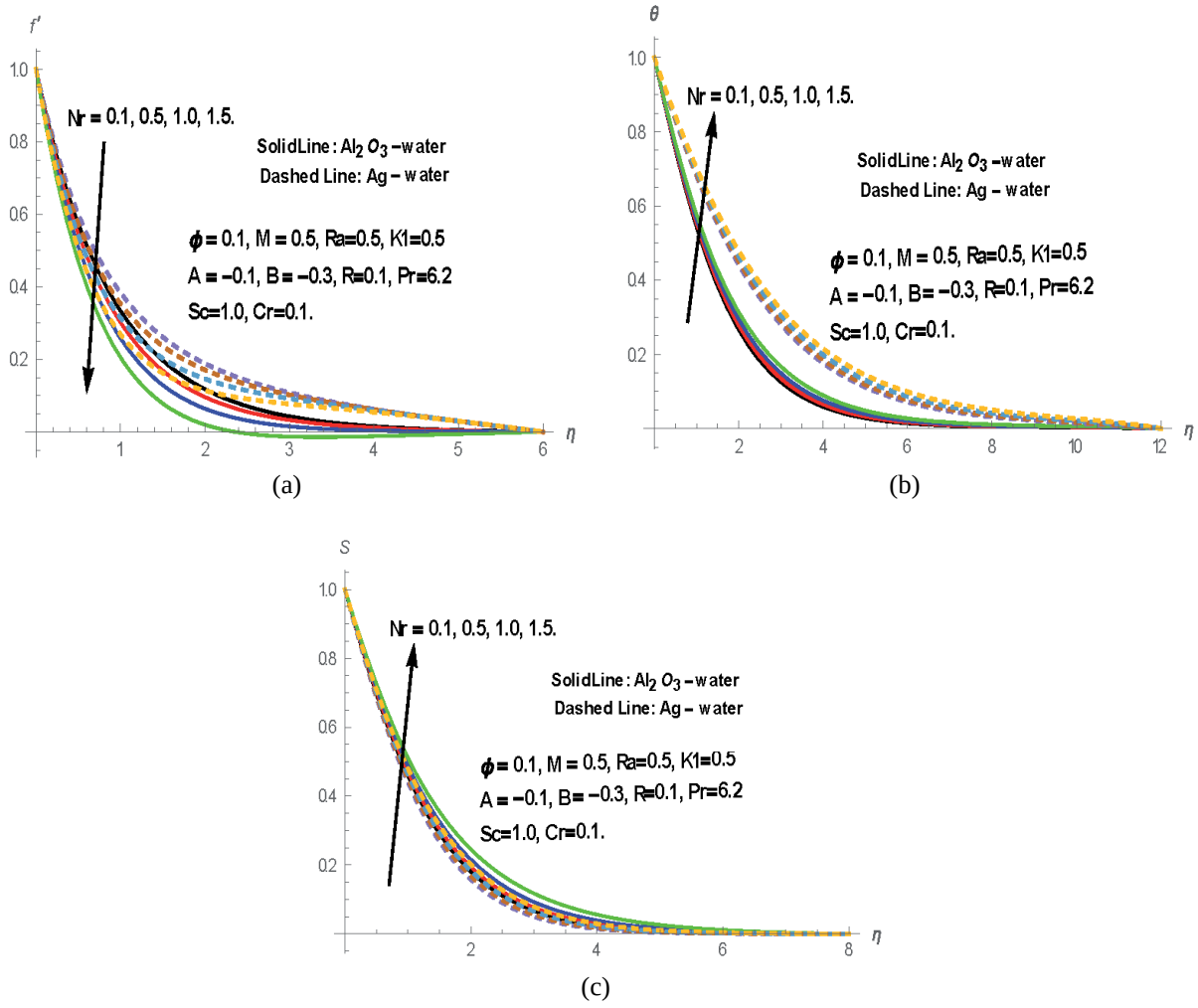

FIG. 4: Effect of Nr on (a) velocity, (b) temperature, and (c) concentration profiles

The values of skin-friction coefficient $(-f''(0))$, local Nusselt number $(-\theta'(0))$, and local Sherwood number $(-\phi'(0))$ for both Al_2O_3–water and Ag–water nanofluid are calculated and presented in Table 3. It is evident that the local skin-friction coefficient enhances whereas dimensionless heat transfer rates decrease in both Al_2O_3–water and Ag–water based nanofluids with increasing values of the magnetic field parameter M. Also, the dimensionless mass transfer rates decelerate in both nanofluids with increasing values of M. It is found that the rate of heat transfer and mass transfer increases in both Al_2O_3–water and Ag–water based nanofluids, but the reverse trend is observed in skin-friction coefficient with the increasing values of nanoparticle volume fraction parameter ε. It is also noted from this table that the rate of change of velocity and temperature retards, whereas the rate of mass transfer increases in both Al_2O_3–water and Ag–water based nanofluids with increasing values of thermal radiation parameter R. It is reported that rate of velocity depreciates whereas dimensionless heat and mass transfer rates rise in both nanofluids with increasing values of chemical reaction parameter Cr. It is also noted from this table that the skin-friction coefficient is impeded but both heat and mass transfer rates escalate with the increasing values of convection parameter Ra in both nanofluids. The value of the skin-friction coefficient escalates, however, and rates of heat and mass transfer decrease with the higher values of buoyancy ratio parameter Nr.

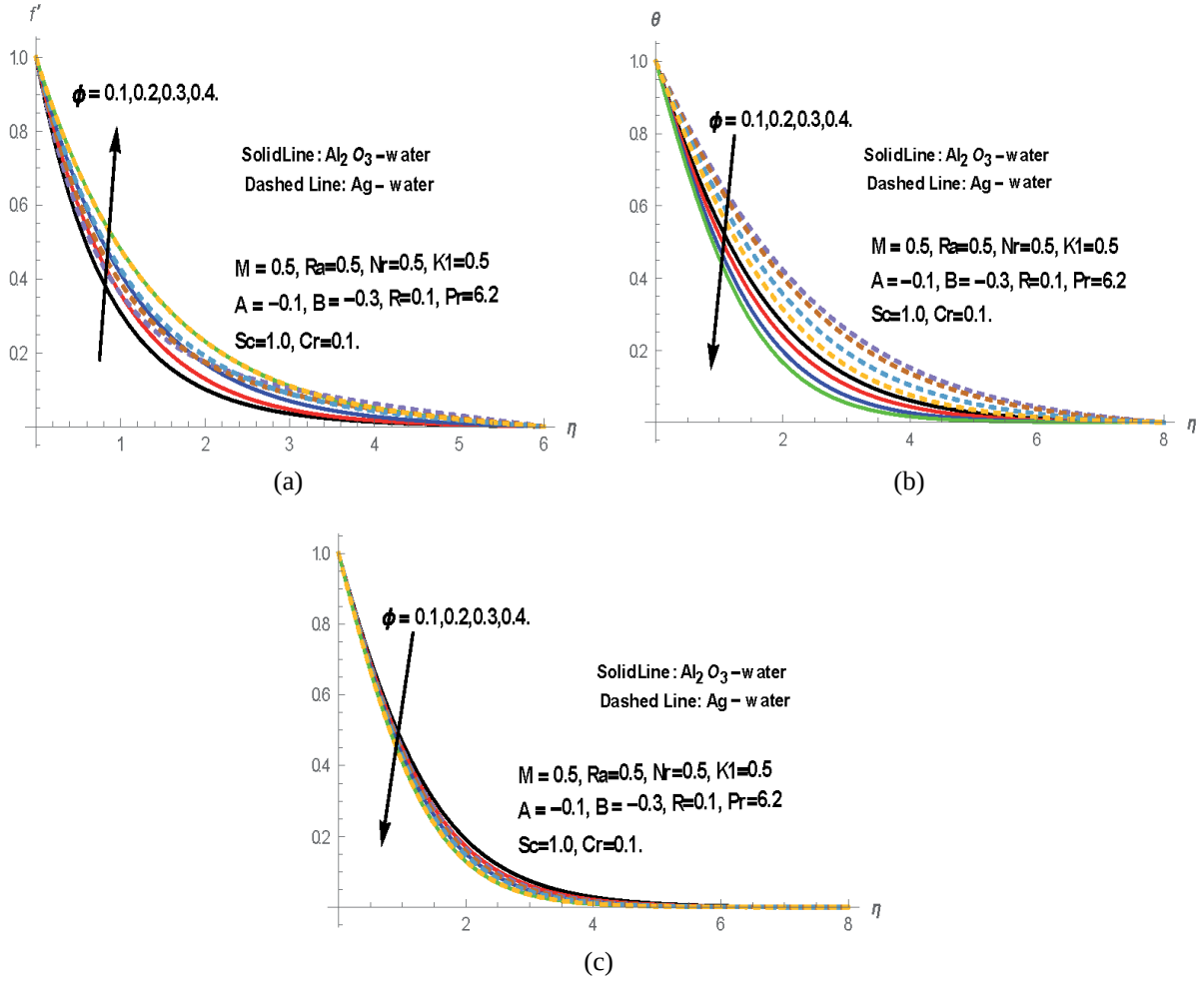

FIG. 5: Effect of φ on (a) velocity, (b) temperature, and (c) concentration profiles

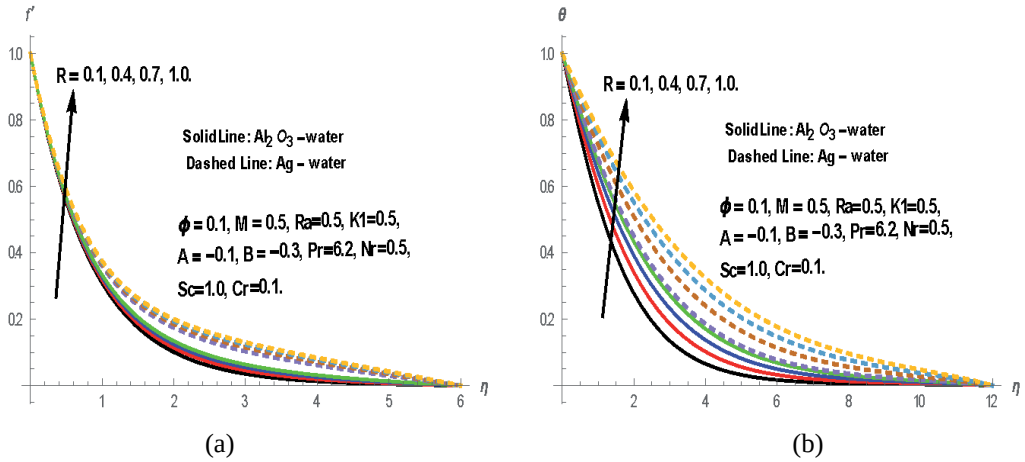

FIG. 6: Effect of R on (a) velocity and (b) temperature profiles

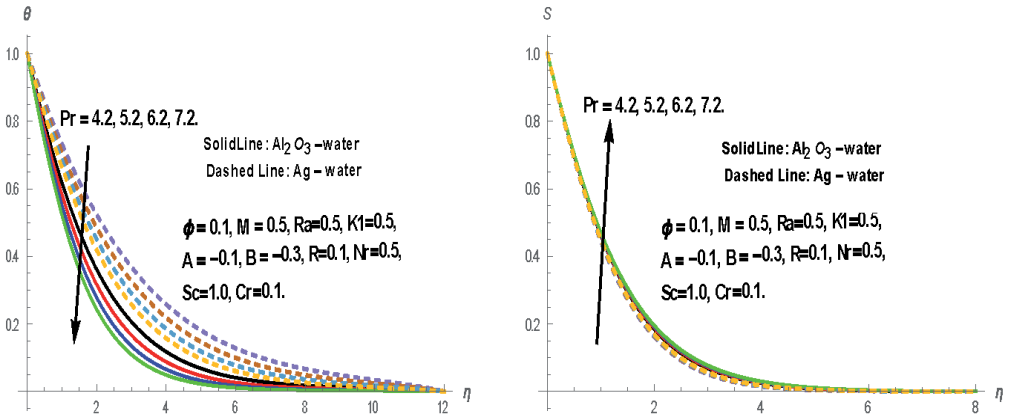

(a) (b)

FIG. 7: Effect of Pr on (a) temperature and (b) concentration profiles

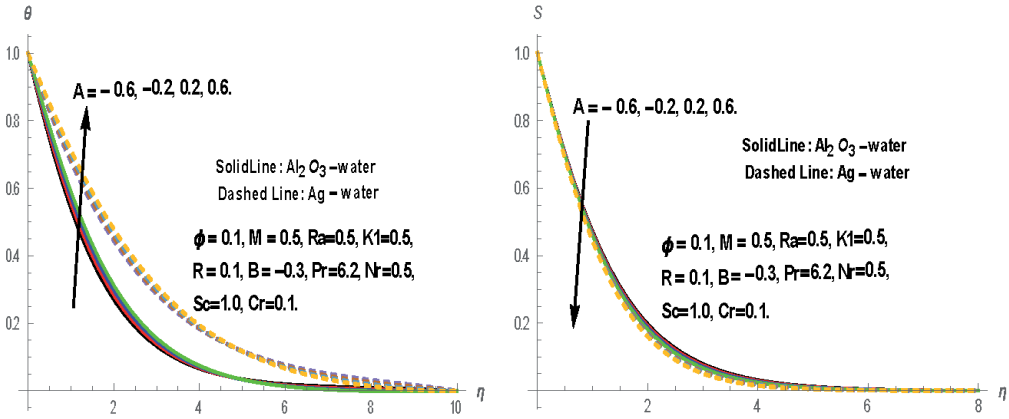

(a) (b)

FIG. 8: Effect of A on (a) temperature and (b) concentration profiles

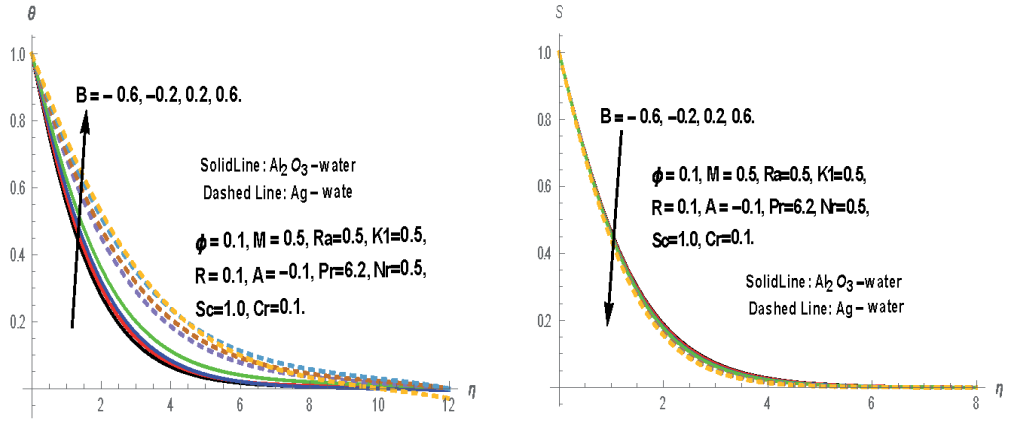

(a) (b)

FIG. 9: Effect of B on (a) temperature and (b) concentration profiles

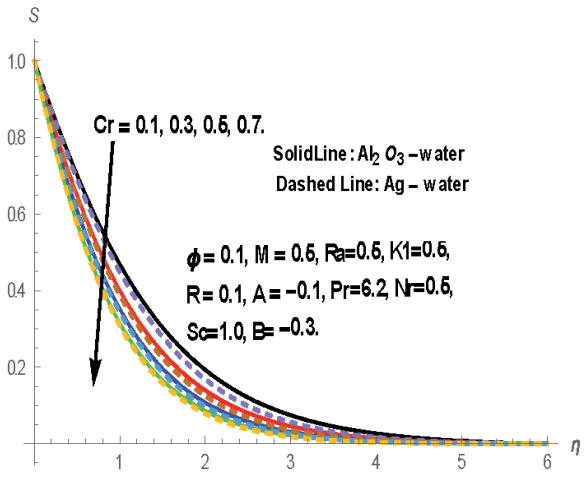

FIG. 10: Effect of Cr on concentration profiles

TABLE 3: Effect of various parameters on local skin-friction coefficient $\left(-f''(0)\right)$, local Nusselt number $(-\theta'(0))$, and local Sherwood number $(-\phi'(0))$ for fixed Pr = 6.2 (water), Sc = 1.0, $A = -0.1$, $B = -0.3$, $k_1 = 0.5$

Parameter						$-f''(0)$		$-\theta'(0)$		$-\phi'(0)$	
M	Φ	R	Cr	Ra	Nr	Al_2O_3	Ag	Al_2O_3	Ag	Al_2O_3	Ag
0.1	0.1	0.1	0.1	0.5	0.5	1.063323	0.992391	0.713517	0.338850	0.661199	0.687919
0.5	0.1	0.1	0.1	0.5	0.5	1.203238	1.146476	0.697888	0.330351	0.641486	0.665458
0.7	0.1	0.1	0.1	0.5	0.5	1.359906	1.316317	0.682070	0.322128	0.620796	0.641753
1.0	0.1	0.1	0.1	0.5	0.5	1.501459	1.467592	0.669197	0.315778	0.603438	0.621880
0.5	0.1	0.1	0.1	0.5	0.5	1.155146	0.936807	0.520045	0.250195	0.653309	0.640110
0.5	0.2	0.1	0.1	0.5	0.5	0.999505	0.868662	0.557877	0.259700	0.672277	0.684939
0.5	0.3	0.1	0.1	0.5	0.5	0.841171	0.827354	0.602697	0.278026	0.696024	0.701148
0.5	0.4	0.1	0.1	0.5	0.5	0.745470	0.742853	0.640306	0.297289	0.712146	0.713179
0.5	0.1	0.1	0.1	0.5	0.5	1.203238	1.146476	0.697888	0.330351	0.641486	0.665458
0.5	0.1	0.3	0.1	0.5	0.5	1.190909	1.138894	0.608389	0.292808	0.646345	0.668602
0.5	0.1	0.5	0.1	0.5	0.5	1.181391	1.133521	0.545141	0.267031	0.650189	0.670820
0.5	0.1	0.7	0.1	0.5	0.5	1.173766	1.129508	0.497634	0.248189	0.653311	0.672469
0.5	0.1	0.1	0.1	0.5	0.5	1.213575	1.155567	0.801117	0.383642	0.639287	0.662466
0.5	0.1	0.1	0.3	0.5	0.5	1.206452	1.149396	0.802641	0.384226	0.792400	0.806975
0.5	0.1	0.1	0.5	0.5	0.5	1.201470	1.144876	0.803619	0.384615	0.917060	0.927587
0.5	0.1	0.1	0.7	0.5	0.5	1.197634	1.141312	0.804322	0.384899	1.025075	1.033281
0.5	0.1	0.1	0.1	0.1	0.5	1.278496	1.268919	0.687572	0.317286	0.628315	0.633765
0.5	0.1	0.1	0.1	0.5	0.5	1.203238	1.146476	0.697888	0.330351	0.641486	0.665458
0.5	0.1	0.1	0.1	1.0	0.5	1.111508	0.999964	0.709687	0.344290	0.656259	0.696570
0.5	0.1	0.1	0.1	1.5	0.5	1.022038	0.859397	0.720489	0.356295	0.669552	0.721958
0.5	0.1	0.1	0.1	0.5	0.1	1.128954	1.074169	0.707194	0.333662	0.653238	0.675311
0.5	0.1	0.1	0.1	0.5	0.5	1.222155	1.164829	0.695419	0.329482	0.638341	0.662863
0.5	0.1	0.1	0.1	0.5	1.0	1.339257	1.277671	0.679042	0.323841	0.617130	0.645912
0.5	0.1	0.1	0.1	0.5	1.5	1.465059	1.396430	0.658552	0.317210	0.589567	0.625725

5. CONCLUSIONS

In the present article, we have analyzed the boundary layer flow and heat and mass transfer characteristics of Al_2O_3–water and Ag–water nanofluids through a porous medium over a vertical cone by taking thermal radiation, magnetic field, time-dependent and temperature-dependent heat source/sink, and chemical reaction effects into consideration. The conservation equations of mass, momentum, energy, and nanoparticle volume concentration together with the boundary conditions are transformed into a set of highly nonlinear ordinary differential equations with the help of similarity transformations. These transformed equations are solved numerically using an extensively validated, highly efficient, most suitable variational FEM. The important conclusions given by the numerical solutions of the problem are as follows.

1. Velocity profiles depreciate, whereas temperature and concentration profiles elevate, with M in both Al_2O_3–water and Ag–water based nanofluids.
2. When the values of φ increase, then the velocity distributions rise, whereas temperature and concentration profiles depreciate in the boundary layer regime.
3. Temperature profiles improve with space dependence (A) and temperature dependence (B) for heat source/sink parameters.
4. As the value of R increases, both velocity and temperature profiles elevate in both the Al_2O_3–water and Ag–water based nanofluids.
5. The concentration profiles are highly influenced by the chemical reaction parameter in the flow region.

ACKNOWLEDGMENT

The authors are very much thankful to the reviewers for their decent suggestions and observations to improve the quality of the manuscript.

REFERENCES

Aminossadati, S.M. and Ghasemi, B., Natural convection cooling of a localised heat source at the bottom of a nanofluid-filled enclosure, *Eur. J. Mech. B*, vol. **28**, pp. 630–640, 2009.

Amit, M. and Mahesh Kumar, S., Convection in magnetic nanofluid in porous media, *J. Porous Media*, vol. **17**, pp. 439–455, 2014.

Anwar Bég, O., Takhar, H.S., Bhargava, R., Rawat, S., and Prasad, V.R., Numerical study of heat transfer of a third grade viscoelastic fluid in non-Darcian porous media with thermophysical effects, *Phys. Scr.*, vol. **77**, pp. 1–11, 2008.

Bhargava, R., Sharma, R., and Bég, O.A., Oscillatory chemically-reacting MHD free convection heat and mass transfer in a porous medium with Soret and Dufour effects: Finite element modeling, *Int. J. Appl. Math. Mech.*, vol. **5**, pp. 15–37, 2009.

Bresme, F. and Oettel, M., Nanoparticles at fluid interfaces, *J. Phys. Condense. Matter*, vol. **19**, 413101, 2007.

Buongiorno, J., Convective transport in nanofluids, *J. Heat Transfer*, vol. **128**, pp. 240–250, 2006.

Chamkha, A.J., MHD flow of a uniformly stretched vertical permeable surface in the presence of heat generation/absorption and a chemical reaction, *Int. Commun. Heat Mass Transfer*, vol. **30**, pp. 413–422, 2003.

Chamkha, A.J. and Rashad, A.M., Unsteady heat and mass transfer by MHD mixed convection flow from a rotating vertical cone with chemical reaction and Soret and Dufour effects, *Can. J. Chem. Eng.*, vol. **92**, pp. 758–767, 2014.

Chamkha, A.J., Abbasbandy, S., Rashad, A.M., and Vajravelu, K., Radiation effects on mixed convection over a wedge embedded in a porous medium filled with a nanofluid, *Transp. Porous Media*, vol. **91**, pp. 261–279, 2012.

Chamkha, A.J., Abbasbandy, S., Rashad, A.M., and Vajravelu, K., Radiation effects on mixed convection about a cone embedded in a porous medium filled with a nanofluid, *Meccanica*, vol. **48**, pp. 275–285, 2013.

Choi, S.U.S., Zhang, Z.G., Yu, W., Lockwood, F.E., and Grulke, E.A., Anomalous thermal conductivity enhancement in nano-tube suspensions, *Appl. Phys. Lett.*, vol. **79**, pp. 2252–2254, 2001.

Eastman, J.A., Choi, S.U.S., Li, S., Thompson, L.J., and Lee, S., Enhanced thermal conductivity through the development of nanofluid, in S. Komarneni, J. C. Parker, H. J. Wollenberger, eds., *Nanophase and Nanocomposite Materials II*, Pittsburg, PA: MRS, pp. 3–11, 1997.

Eastman, J.A., Choi, S.U.S., Li, S., Yu, W., and Thompson, L.J., Anomalously increased effective thermal conductivities of ethylene glycol-based nano-fluids containing copper nano-particles, *Appl. Phys. Lett.*, vol. **78**, pp. 718–720, 2001.

Eliodoro, C. and Pietro, A., Enhancing surface heat transfer by carbon nanofins: Towards an alternative to nanofluids?, *Nanoscale Res. Lett.*, vol. **6**, p. 249, 2011.

Eliodoro, C., Matteo, F., Pietro, A., and Paolo, D., Scaling behaviour for the water transport in nanoconfined geometries, *Nat. Commun.*, vol. **5**, p. 4564, 2014.

EL-Kabeir, S.M.M., Modather, M., and Rashad, A.M., Effect of thermal radiation on mixed convection flow of a nanofluid about a solid sphere in a saturated porous medium under convective boundary condition, *J. Porous Media*, vol. **18**, pp. 569–584, 2015.

Ellahi, R., The effects of MHD and temperature dependent viscosity on the flow of non-Newtonian nanofluid in a pipe: Analytical solutions, *Appl. Math. Model.*, vol. **37**, pp. 1451–1457, 2013.

Ellahi, R., Raza, M., and Vafai, K., Series solutions of non-Newtonian nanofluids with Reynolds' model and Vogel's model by means of the homotopy analysis method, *Math. Comput. Modell.*, vol. **55**, pp. 1876–1891, 2012.

Ellahi, R., Aziz, S., and Zeeshan, A., Non Newtonian nanofluids flow through a porous medium between two coaxial cylinders with heat transfer and variable viscosity, *J. Porous Media*, vol. **16**, pp. 205–216, 2013.

Ellahi, R., Hassan, M., and Zeeshan, A., Shape effects of nanosize particles in Cu–H_2O nanofluid on entropy generation, *Int. J. Heat Mass Transfer*, vol. **81**, pp. 449–456, 2015a.

Ellahi, R., Hassan, M., and Zeeshan, A., Study on magnetohydrodynamic nanofluid by means of single and multi-walled carbon nanotubes suspended in a salt water solution, *IEEE Trans. Nanotechnol.*, vol. **14**, pp. 726–734, 2015b.

Fakhreddine Segni, O. and Rachid, B., Heterogeneous nanofluids: Natural convection heat transfer enhancement, *Nanoscale Res. Lett.*, vol. **6**, p. 222, 2011.

Ghasemi, B. and Aminossadati, S.M., Brownian motion of nanoparticles in a triangular enclosure with natural convection, *Int. J. Thermal Sci.*, vol. **49**, pp. 931–940, 2010.

Haddad, Z., Oztop, H.F., Abu-Nada, E., and Mataoui, A., A review on natural convective heat transfer of nanofluids, *Renew. Sust. Energ Rev.*, vol. **16**, pp. 5363–5378, 2012.

Hamad, M.A.A., Analytical solution of natural convection flow of a nanofluid over a linearly stretching sheet in the presence of magnetic field, *Int. Commun. Heat Mass Transfer*, vol. **38**, pp. 487–492, 2011.

Ho, C.J., Liu, W.K., Chang, Y.S., and Lin, C.C., Natural convection heat transfer of alumina–water nanofluid in vertical square enclosures: An experimental study, *Int. J. Thermal Sci.*, vol. **49**, pp. 1345–1353, 2010.

Kamyar, A., Saidur, R., and Hasanuzzaman, M., Application of computational fluid dynamics (CFD) for nanofluid, *Int. J. Heat Mass Transfer*, vol. **55**, pp. 4104–4115, 2012.

Khanafer, K., Vafai, K., and Lightstone, M., Buoyancy-driven heat transfer enhancement in a two dimensional enclosure utilizing nanofluids, *Int. J. Heat Mass Transfer*, vol. **46**, pp. 3639–3653, 2003.

Kuznetsov, A.V. and Nield, D.A., Natural convective boundary-layer flow of a nanofluid past a vertical plate, *Int. J. Thermal Sci.*, vol. **49**, pp. 243–247, 2010.

Lervik, A., Bresme, F., and Kjelstrup, S., Heat transfer in soft nanoscale interfaces: The influence of interface curvature, *Soft Matter*, vol. **12**, pp. 2407–2414, 2009.

Li, C.H. and Peterson, G.P., Experimental studies of natural convection heat transfer of Al_2O_3/DI water nanoparticle suspensions (nanofluids), *Adv. Mech. Eng.*, vol. **02**, 742739, 2010.

Nnanna, A.G.A., Experimental model of temperature-driven nanofluid, *J. Heat Transfer*, vol. **129**, pp. 697–704, 2007.

Noreen Sher, A., Raja, M., and Ellahi, R., Influence of heat generation and heat flux in peristalsis with interaction of nanoparticles, *Eur. Phys. J. Plus*, vol. **129**, p. 185, 2014a.

Noreen Sher, A., Rahman, S.U., Ellahi, R., and Nadeem, S., Nano fluid flow in tapering stenosed arteries with permeable walls, *Int. J. Thermal Sci.*, vol. **85**, pp. 54–61, 2014b.

Noreen Sher, A., Raja, M., and Ellahi, R., Influence of induced magnetic field and heat flux with the suspension of carbon nanotubes for the peristaltic flow in a permeable channel, *J. Magnetism Magnetic Mater.*, vol. **381**, pp. 405–415, 2015.

Oztop, H.F. and Abu-Nada, E., Numerical study of natural convection in partially heated rectangular enclosure filled with nanofluids, *Int. J. Heat Fluid Flow*, vol. **29**, pp. 1326–1336, 2008.

Putra, N., Roetzel, W., and Das, S.K., Natural convection of nano-fluids, *Heat Mass Transfer*, vol. **39**, pp. 775–784, 2003.

Rana, P. and Bhargava, R., Flow and heat transfer of a nanofluid over a nonlinearly stretching sheet: A numerical study, *Commun. Nonlinear Sci. Numer. Simul.*, vol. **17**, pp. 212–226, 2012.

Rashad, A.M., Abbasbandy, S., and Chamkha, A.J., Non-Darcy natural convection from a vertical cylinder embedded in a thermally stratified and nanofluid-saturated porous media, *ASME J. Heat Transfer*, vol. **136**, 22503-1-9, 2014.

Rashidi, S., Dehghan, M., Ellahi, R., Riaz, M., and Jamal-Abad, M.T., Study of stream wise transverse magnetic fluid flow with heat transfer around a porous obstacle, *J. Magnetism Magnetic Mater.*, vol. **378**, pp. 128–137, 2015.

Reddy, P.S. and Chamkha, A.J., Soret and Dufour effects on MHD convective flow of Al_2O_3–water and TiO_2–water nanofluids past a stretching sheet in porous media with heat generation/absorption, *Adv. Powder Technol.*, vol. **27**, pp. 1207–1218, 2016.

Rui, N., Sheng-Qi, Z., and Ke-Qing, X., An experimental investigation of turbulent thermal convection in water-based alumina nanofluid, *Phys. Fluid*, vol. **23**, 022005, 2011.

Sarkar, J., A critical review on convective heat transfer correlations of nanofluids, *Renew. Sust. Energy Rev.*, vol. **15**, pp. 3271–3277, 2011.

Sheikholeslami, M. and Ellahi, R., Three dimensional mesoscopic simulation of magnetic field effect on natural convection of nanofluid, *Int. J. Heat Mass Transfer*, vol. **89**, pp. 799–808, 2015.

Sheikholeslami, M., Ellahi, R., Mohsan, H., and Soheil, S., A study of natural convection heat transfer in a nanofluid filled enclosure with elliptic inner cylinder, *Int. J. Numer. Methods Heat Fluid Flow*, vol. **24**, pp. 1906–1927, 2014a.

Sheikholeslami, M., Ellahi, R., Ashorynejad, H.R., Domairry, G., and Hayat, T., Effects of heat transfer in flow of nanofluids over a permeable stretching wall in a porous medium, *J. Comput. Theoret. Nanosci.*, vol. **11**, pp. 486–496, 2014b.

Sheikholeslami, M., Bandpy, M.G., Ellahi, R., and Zeeshan, A., Simulation of CuO–water nanofluid flow and convective heat transfer considering Lorentz forces, *J. Magnetism Magnetic Mater.*, vol. **369**, pp. 69–80, 2014c.

Sheikholeslami, M., Ganji, D.D., Younus Javed, M., and Ellahi, R., Effect of thermal radiation on nanofluid flow and heat transfer using two phase model, *J. Magnetism Magnetic Mater.*, vol. **374**, pp. 36–43, 2015a.

Sheikholeslami, M., Noreen Sher, A., and Mustafac, M.T., Simulation of ferrofluid flow for magnetic drug targeting using Lattice Boltzmann method, *Z. Naturforsch. Aü* , vol. **70**, pp. 115–124, 2015b.

Sheremet, M.A. and Pop, I., Conjugate natural convection in a square porous cavity filled by a nanofluid using Buongiorno's mathematical model, *Int. J. Heat Mass Transfer*, vol. **79**, pp. 137–145, 2014.

Sheremet, M.A., Pop, I., and Rahman, M.M., Three-dimensional natural convection in a porous enclosure filled with a nanofluid using Buongiorno's mathematical model, *Int. J. Heat Mass Transfer*, vol. **82**, pp. 396–405, 2015a.

Sheremet, M.A., Grosan, T., and Pop, I., Free convection in a square cavity filled with a porous medium saturated by nanofluid using Tiwari and Das' nanofluid model, *Transp. Porous Media*, vol. **106**, pp. 595–610, 2015b.

Sheremet, M.A., Grosan, T., and Pop, I., Natural convection in a cubical porous cavity saturated with nanofluid using Tiwari and Das' nanofluid model, *J. Porous Media*, vol. **18**, pp. 585–596, 2015c.

Ternik, P. and Rudolf, R., Heat transfer enhancement for natural convection flow of water-based nanofluids in a square enclosure, *Int. J. Simul. Modell.*, vol. **11**, pp. 29–39, 2012.

Wang, X.Q. and Mujumdar, A.S., A review on nanofluids—Part 2: Experiments and applications, *Braz. J. Chem. Eng.*, vol. **25**, pp. 631–648, 2008.

Wen, D. and Ding, Y., Formulation of nanofluids for natural convective heat transfer applications, *Int. J. Heat Fluid Flow*, vol. **26**, pp. 855–864, 2005.

Xie, H., Wang, J., Xi, T., Liu, Y., Ai, F., and Wu, Q., Thermal conductivity enhancement of suspensions containing nanosized alumina particles, *J. Appl. Phys.*, vol. **91**, pp. 4568–4572, 2002.

Zeeshan, A., Ellahi, R., and Hassan, M., Magnetohydrodynamic flow of water/ethylene glycol based nanofluids with natural convection through porous medium, *Eur. Phys. J. Plus*, vol. **129**, p. 261, 2014.